BBA - Molecular Basis of Disease 1864 (2018) 3164–3180

Contents lists available at ScienceDirect

BBA - Molecular Basis of Disease

journal homepage: www.elsevier.com/locate/bbadis

PERK inhibition attenuates the abnormalities of the secretory pathway and the increased apoptotic rate induced by *SIL1* knockdown in HeLa cells

Vanessa Capone[a,b], Emanuela Clemente[a,b], Elena Restelli[c], Antonella Di Campli[d], Samantha Sperduti[a,b], Francesca Ornaghi[c], Laura Pietrangelo[b,e], Feliciano Protasi[b,f], Roberto Chiesa[c], Michele Sallese[a,b,*]

[a] Department of Medical, Oral and Biotechnological Sciences, University G. d'Annunzio, Chieti 66100, Italy
[b] CeSI-MeT, Centre for Research on Ageing and Translational Medicine, University G. d'Annunzio, Chieti 66100, Italy
[c] Department of Neuroscience, IRCCS - Mario Negri Institute for Pharmacological Research, Via G. La Masa 19, 20156 Milan, Italy
[d] Institute of Protein Biochemistry, National Research Council, Naples, Italy
[e] DNISC, Dept. of Neuroscience, Imaging, and Clinical Sciences, University G. d'Annunzio, Chieti, 66100, Italy
[f] DMSI, Dept. of Medicine and Aging Science, University G. d'Annunzio, Chieti, 66100, Italy

ARTICLE INFO

Keywords:
Marinesco-Sjögren syndrome
SIL1
Membrane trafficking
Cell survival

ABSTRACT

Loss-of-function mutations in the *SIL1* gene are linked to Marinesco-Sjögren syndrome (MSS), a rare multisystem disease of infancy characterized by cerebellar and skeletal muscle degeneration. SIL1 is a ubiquitous adenine nucleotide exchange factor for the endoplasmic reticulum (ER) chaperone BiP. The complexity of mechanisms by which loss of SIL1 causes MSS is not yet fully understood. We used HeLa cells to test the hypothesis that impaired protein folding in the ER due to loss of SIL1 could affect secretory trafficking, impairing the transport of cargoes essential for the function of MSS vulnerable cells. Immunofluorescence and ultrastructural analysis of SIL1-knocked-down cells detected ER chaperone aggregation, enlargement of the Golgi complex, increased autophagic vacuoles, and mitochondrial swelling. SIL1-interefered cells also had delayed ER-to-plasma membrane transport with retention of Na^+/K^+-ATPase and procollagen-I in the ER and Golgi, and increased apoptosis. The PERK pathway of the unfolded protein response was activated in SIL1-interfered cells, and the PERK inhibitor GSK2606414 attenuated the morphological and functional alterations of the secretory pathway, and significantly reduced cell death. These results indicate that loss of SIL1 is associated with alterations of secretory transport, and suggest that inhibiting PERK signalling may alleviate the cellular pathology of *SIL1*-related MSS.

1. Introduction

Marinesco-Sjögren syndrome (MSS) is a rare, early-onset, autosomal recessive genetic disease (MIM 248800) causing cataracts, cerebellar ataxia, hypotonia, dysarthria, short stature, and mental retardation ranging from mild to severe [1–4]. Clinical signs appear in early infancy, and progress for a number of years; then they stabilise and patients live to old age. There is no therapy for MSS, and medical care is mainly symptomatic, with educational and rehabilitative programs to improve walking, cognition and speaking.

Approximately 60% of MSS cases are linked to loss-of-function mutations in the *SIL1* gene [3,4]. The SIL1 protein is an endoplasmic reticulum (ER) ATPase exchange factor that assists in the release of ADP from the essential chaperone BiP, also known as GRP78 [5]. BiP plays vital roles in the translocation of newly synthesized proteins into the ER lumen, in the ion gating of the aqueous pore translocon, in protein folding, and in the retrotranslocation of misfolded proteins targeted to ER-associated degradation (ERAD) [6–8]. BiP also participates in activating the unfolded protein response (UPR), a complex signalling pathway triggered by the accumulation of unfolded/misfolded proteins in the ER, whose purposes are to restore proteostasis by boosting the ER protein-folding capacity, reduce the load of newly synthesized proteins entering the ER, and degrade the unfolded proteins [9].

The UPR signals through three distinct ER transmembrane protein sensors: inositol-requiring enzyme 1 (IRE1), protein kinase RNA (PKR)-like ER kinase (PERK), and activating transcription factor 6 (ATF6). Under normal conditions these sensors are inactive due to BiP's association with their luminal domains [10–13]. When the level of unfolded proteins in the ER rises, BiP dissociates from the ER stress sensors to bind to exposed hydrophobic regions of unfolded proteins, enabling

* Corresponding author at: Department of Medical, Oral and Biotechnological Sciences, University G. d'Annunzio, Chieti 66100, Italy.
E-mail address: michele.sallese@unich.it (M. Sallese).

https://doi.org/10.1016/j.bbadis.2018.07.003
Received 16 January 2018; Received in revised form 5 June 2018; Accepted 3 July 2018
Available online 07 July 2018

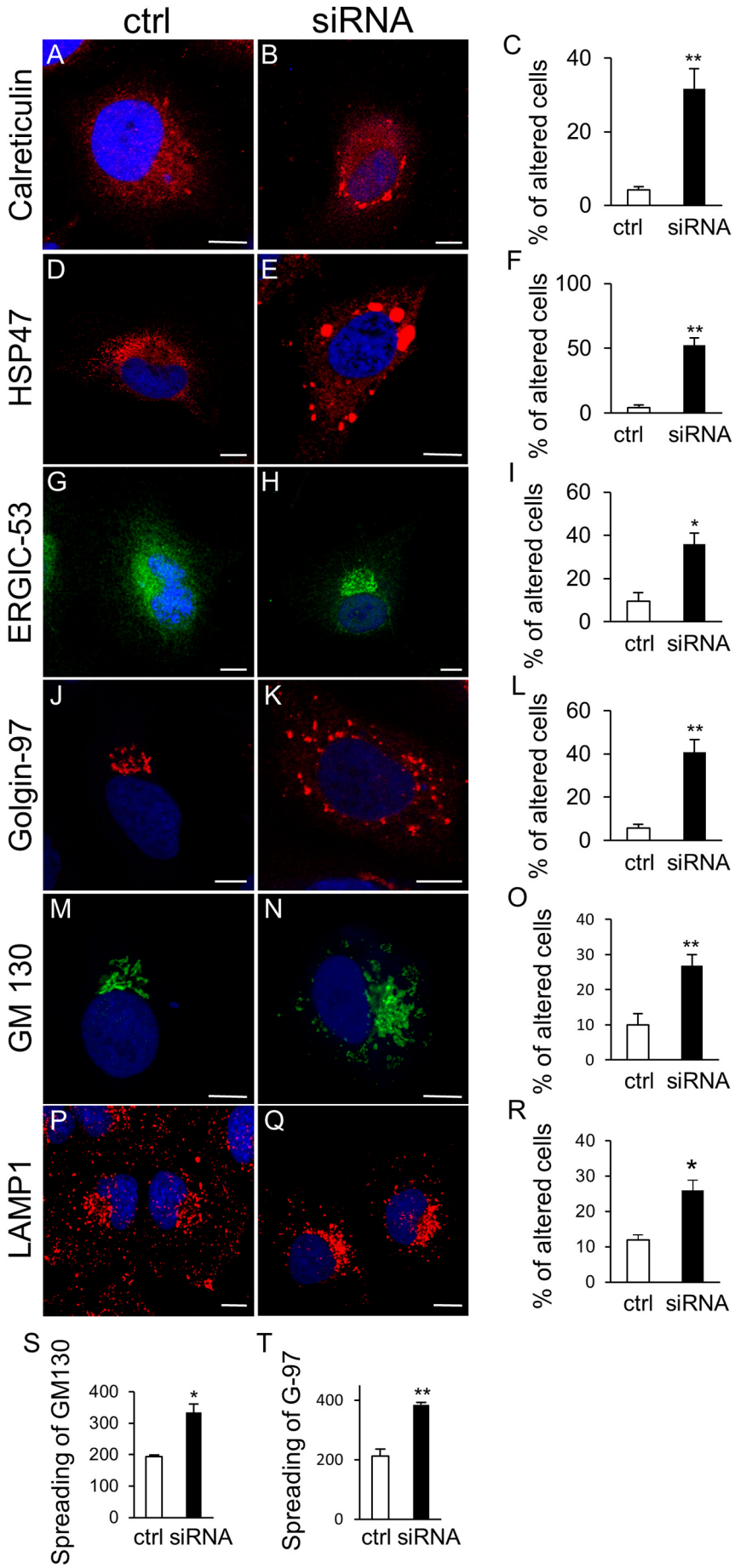

(caption on next page)

Fig. 1. Organelle morphology is altered in SIL1 KD HeLa cells. HeLa cells were transfected with ctrl or SIL1 (S20) siRNA. After 72 h they were fixed and stained for calreticulin, HSP47, ERGIC-53, Golgin-97, GM130 and LAMP1 (red) in combination with DRAQ5 (blue) to identify the cell nuclei. Scale bars, 10 μm. The percentage of cells showing altered marker distribution (C, F, I, L, O and R) was quantified. The extension of the Golgi complex (S and T) is expressed in arbitrary units (AU). Data are the mean ± SEM of three independent experiments. $^{**}p < 0.01$, $^{*}p < 0.05$ versus control by Student's *t*-test. G-97, golgin-97.

IRE1 and PERK dimerization and autophosphorylation, and unmasking a Golgi localization signal of ATF6 (Supplemental Fig. S1). Activated IRE1 initiates the unconventional splicing of the mRNA encoding the transcriptional factor X-box-binding protein 1 (XBP1) to produce the more stable form sXBP1 with a potent transactivator domain that enhances transcription of genes involved in protein folding, secretion and ERAD [14]. IRE1 also triggers a more conventional signal transduction cascade leading to JNK activation, which controls autophagy and cell death (Supplemental Fig. S1) [15,16]. On arrival at the Golgi, ATF6 is cleaved by site 1 and 2 proteases, releasing a cytosolic domain which translocates to the nucleus and induces expression of molecular chaperones and XBP1 (Supplemental Fig. S1). Therefore the IRE1 and ATF6 signalling pathways merge through regulation of XBP1 activity [17]. Activated PERK phosphorylates the α subunit of eukaryotic translation initiation factor 2 (eIF2α). This inhibits protein translation, reducing the overload of misfolded proteins. Some specific mRNAs, however, are preferentially translated during eIF2α-P-mediated translational attenuation. These include the transcription factor ATF4, which upregulates growth arrest and DNA-damage-inducible protein-34 (GADD34), the regulatory subunit of the serine/threonine protein phosphatase 1, which dephosphorylates eIF2α-P, providing a negative feedback mechanism that contributes to rapidly restoring protein synthesis upon resolution of ER stress. If cells are unable to handle the unfolded protein load, protracted ATF4 synthesis induces expression of C/EBP homologous protein (CHOP), which triggers apoptosis. Thus, persistent ER stress eventually leads to cell death.

UPR markers, including CHOP, are up-regulated in degenerating Purkinje cells (PCs) and skeletal muscle fibres in the woozy mouse model of MSS [18,19], suggesting that maladaptive UPR may play a pathogenic role. However, genetic ablation of CHOP did not prevent neurodegeneration in woozy mice [20], indicating that ER stress-induced apoptosis may not be the final executor of cell death. It is also not clear why only skeletal muscle fibres and PCs of cerebellar lobules I-VIII degenerate, whereas PCs of lobules IX and X and other cells of the nervous system or other tissues where SIL1 is also highly expressed do not. The SIL1 homologous 150-kDa oxygen-regulated protein (ORP150; also known as GRP170), can substitute for the SIL1 nucleotide exchange function [20,21], suggesting that the spared tissues may have higher ORP150 levels. However, no major differences in ORP150 expression were found between resistant and vulnerable tissues of woozy mice [22; and our unpublished observations]. Moreover, ORP150 expression is higher in vulnerable than in resistant PCs, but this is not enough to prevent their death, unless ORP150 is transgenically over-expressed [20]. Thus, other factors may contribute to selective cell death in MSS, such as increased ataxin-10 expression, as recently suggested [23].

Ultrastructural analysis of patients' and woozy skeletal muscles showed perturbed organization of the nuclear envelope, widening and proliferation of Golgi and ER membranes, and swelling of mitochondria [19,24–27]. Morphological abnormalities of the nuclear envelope and mitochondria were also reported in SIL1-depleted human embryonic kidney HEK293 cells and in patient derived lymphoblastoid cells [23,24]. Proteomic analysis of these cells brought to light alterations in a number of different intracellular compartments, including the nucleus, the nuclear envelop, the endomembrane system, the mitochondria, the cytoplasm and the cytoskeleton [23,24]. Furthermore, there are indications that these changes affect vesicular transport [24].

In the present study, we explored the hypothesis that non-optimal ER folding activity might lead to impaired production and transport of membrane or soluble proteins essential for correct function and survival of MSS vulnerable cells. As a first approach to test this, we analysed the morphology and function of the secretory pathway in cervical carcinoma HeLa cells, in which loss of SIL1 was modelled by RNAi-mediated gene silencing. SIL1 knockdown (KD) preferentially activated the PERK branch of the UPR. SIL1 KD cells showed ER chaperone aggregation, and morphological and functional alterations of the secretory pathway, with intracellular retention of proteins potentially important for neuronal and muscle physiology. SIL1 KD significantly raised the apoptotic rate, and the PERK inhibitor GSK2606414 partially rescued the morphological and functional alterations of the secretory pathway and significantly reduced cell death.

These results indicate that impairment of secretory transport may contribute to the pathogenesis of MSS, and suggest that inhibiting PERK signalling may alleviate the cellular pathology caused by loss of SIL1.

2. Materials and methods

2.1. Reagents

The following antibodies were used: mouse anti-HSP47 monoclonal, mouse anti-CHOP monoclonal, mouse anti-Na^+/K^+-ATPase alpha1 monoclonal, rabbit anti-ERGIC-53 polyclonal (Santa Cruz Biotechnology); rabbit anti-GAPDH polyclonal (Cell Signaling Technology); rabbit anti-TGN46 polyclonal, rabbit anti-HSP47 polyclonal, rabbit anti-PC-I polyclonal (Novus Biologicals); rabbit anti-actin polyclonal, mouse prestige anti-SIL1, mouse P5D4 anti-VSVG monoclonal (Sigma Aldrich); mouse anti-Golgin 97 monoclonal (Life Biotechnology); mouse anti-RAB5 monoclonal, mouse anti-GM130 monoclonal, mouse anti-BiP monoclonal (BD transduction Laboratories); rabbit anti-PDI polyclonal, mouse anti-LAMP1 monoclonal (Abcam); mouse anti-calreticulin monoclonal (Stressgene); mouse anti-PC-I monoclonal (Developmental Studies Hybridoma Bank, Iowa University); polyclonal rabbit antibodies against SEC31 and GM130 were kindly provided by A. De Matteis and G. Di Tullio. Anti-mouse and rabbit IgG secondary antibodies were Alexa 488 and Alexa 546 (Molecular Probes, OR, USA), and Cy3-conjugated (Sigma-Aldrich).

All reagents were of analytical grade or higher (Sigma, unless otherwise specified). DRAQ5 was from Life Technologies. GSK2606414 was from Calbiochem. SIL1 siRNA sequences were as follows: siRNA2 (S2) UUUCAAAUUAUUUCGGAACUUGUCCUC and siRNA20 (S20) CGUACCAUGAUCUGCAUGUCAGUCUCA from Integrated DNA technology (IDT); siRNA3 (S3) code SASI_Hs01_00196801 was from Sigma-Aldrich. Control siRNA were universal negative control #1 from Sigma-Aldrich and negative control DS NC1 from IDT. Most of the experiments were done with at least two different targeting siRNAs, producing similar results.

2.2. Cells

Human HeLa and SH-SY5Y cells were maintained respectively in Dulbecco's modified Eagle's medium and minimum essential medium, supplemented with 10% foetal calf serum, 2 mM L-glutamine, 100 μg/mL streptomycin sulphate, and 100 units/mL penicillin G (Gibco BRL, UK), at 37 °C in a humidified 5% CO_2/air atmosphere. The cells were interfered with HiPerFect (Qiagen), according to the manufacturer's instructions. HeLa and SH-SY5Y cells were stably interfered for SIL1 using the GIPZ lentiviral shRNA particles from Thermo Fisher Scientific (cat. n° VGH5518; targeted sequence CCAGAGAAGCTGCAGCAGT), according to the manufacturer's instructions, and selected with puromycin. Cell viability was evaluated by MTT ([3-(4,5-dimethylthiazol-2-yl)-2,5-diphenyl tetrazolium bromide]) assay as previously

described [28]. Apoptosis was measured by TUNEL assay using the commercially available ApopTag® Peroxidase Apoptosis Detection kit according to the manufacturer's specifications (Millipore). The release of LDH was measured using the Cyto Tox 96 kit (Promega), following the manufacturer's instructions.

2.3. VSV infection and transport pulse protocol

Cells were infected with VSV and VSVG transport was analysed as previously described [29]. Cycloheximide (Sigma Aldrich, WI, USA) was added at 50 μg/mL at the temperature shift.

2.4. RT-qPCR

Total RNA was extracted with trizol reagent (Invitrogen). One microgram of RNA was reverse transcribed using the superscript kit (Invitrogen) according to the manufacturer's instructions. Four and 10 ng of cDNA were amplified by Real-Time PCR System from Applied Biosystems. Primer sequences (IDT) were as follows: sXBP1 forward TGCTGAGTCCGCAGCAGGTG, reverse GCTGGCAGGCTCTGGGGAAG; ATF4 forward TTGAGGATAGTCAGGAGCGT, reverse TGGAACACACA GCTACAGCA; BiP forward CGAGGAGGAGGACAAGAAGG, reverse CACCTTGAACGGCAAGAAT. Data were calculated as the fold change compared to controls, using the $2^{(-\text{Delta Delta Ct})}$ method, with actin as housekeeping control gene for normalization. Gene expression analysis aimed at identifying the molecular pathways possibly involved in cell death was performed with the RT^2 Profiler™ PCR Array Human Cell Death Pathway Finder (Qiagen) according to the manufacturer's instructions.

2.5. Protein analysis

Cells were washed three times with ice-cold 0.9% NaCl and harvested immediately in lysis buffer (1% Triton X-100, 0.1% sodium deoxycholate, 0.1% sodium dodecyl sulphate, 20 mM Tris-HCl, pH 8.0, 150 mM NaCl, 1 mg/mL Na_3VO_4, 5 mM PMSF, 5 μg/mL each of leupeptin, aprotinin, pepstatin), at 4 °C. The cell lysates were centrifuged at 15,000 × *g* for 5 min at 4 °C, to pellet and remove the nuclei. The postnuclear supernatant was immediately processed for SDS-PAGE and Western blotting.

2.6. Fluorescence immunostaining and confocal microscopy

Cells were washed with PBS, fixed in 4% paraformaldehyde (Sigma Aldrich) for 10 min at room temperature and incubated in blocking solution (0.05% saponin, 0.5% bovine serum albumin and 50 mM NH_4Cl in PBS) for 30 min at room temperature. The cells were then incubated with the primary antibodies diluted in blocking solution, for 2–3 h at room temperature, or overnight at 4 °C, then washed three times in PBS and incubated with a fluorescent conjugated anti-IgG secondary antibody for 1 h at room temperature. Cells were examined under a confocal microscope (Zeiss LSM 510 or LSM 800 with airy scan; Zeiss, Thornwood, NY, USA). To quantify the colocalization of the fluorescence signals, the area of interest was delineated manually and the fluorescence intensity or the weighted colocalization coefficient [30] were quantified using LSM510-3.2 and Zen 2.3 software (Zeiss).

2.7. Electron microscopy

Approximately 2×10^6 cells cultured in monolayers were prepared for EM as follows. Cells were detached from the dish with trypsin, centrifuged at 180 × *g* for 2.5 min, washed three times with PBS at 37 °C, fixed with 3.5% glutaraldehyde in 0.1 M NaCaCO buffer for 1 h and stored at 4 °C. For embedding, cells were post-fixed in 2% OsO_4 in the same buffer for 2 h and block-stained in saturated uranyl acetate. After dehydration, specimens were embedded in epoxy resin (Epon 812). Ultrathin sections were cut using a Leica Ultracut R microtome (Leica Microsystem, Austria) with a Diatome knife (Diatome Ltd. CH-2501 Biel, Switzerland) and double-stained with uranyl acetate and lead citrate. Sections were viewed and photographed in a Morgagni Series 268D electron microscope (FEI Company, Brno, Czech Republic) equipped with a Megaview III digital camera and Analy-SIS software (Olympus Soft Imaging Solutions).

Quantitative analysis was done on random micrographs of HeLa and SH-SY5Y cell cultures (vehicle-treated ctrl, ctrl treated with GSK2606414, vehicle-treated SIL1 KD and SIL1 KD treated with GSK2606414). The percentages of cells with accumulation of vacuoles delimited by membranes and containing electron-dense material were determined in micrographs taken at either 5600 or 7100 of magnification (sample size 20 cells/group). The numbers of Golgi stacks in each cell were counted in micrographs taken at 5600/7100 magnification (sample size 20 cells/group). The number of elements forming each stack was determined in micrographs taken at 14,000/18,000 magnification (sample size 20 stacks/group). The width of the cis and trans Golgi cisternae were also measured in the same set of micrographs for each specimen. The mitochondria/area were counted in micrographs taken at 14,000/18,000 magnification and reported as average number per 100 μm^2 (sample size 20 cells/group). In the same set of micrographs mitochondrial average size was determined and expressed as $\mu m^2 \times 10^{-1}$ (HeLa cells sample size: vehicle-treated ctrl, 321 measurements; vehicle-treated SIL1 KD, 203 measurements; SIL1 KD treated with GSK2606414, 317 measurements; SH-SY cells sample size: vehicle-treated ctrl, 98 measurements; ctrl treated with GSK2606414, 127 measurements, vehicle-treated SIL1 KD, 248 measurements; SIL1 KD treated with GSK2606414, 68 measurements).

2.8. Flow cytometry analysis

Cells were fixed in 70% cold ethanol, stained with 50 μg/mL propidium iodide (PI) in PBS containing 200 μg/mL RNase, and acquired using a FACSCantoII flow cytometer equipped with FACSDiVa software (BD Biosciences). Debris were excluded from the analysis after gating them out by setting the forward scatter versus side scatter plot on the viable cells area. Cell doublets and aggregates were excluded by gating FL2-area versus FL2-width. The low flow rate mode (400–500 events s^{-1}) was used to record 20,000 non-debris events for each sample. PI fluorescence data were collected using the linear amplification mode. Cell cycle analysis was done using FCS Express 5 Plus Research Edition. Cells with a DNA content less than 2n ('sub-G0/G1 cells') were considered apoptotic. FACSDiVa software (BD Biosciences) was used for sample analysis. Apoptotic cell death was also evaluated by Annexin V staining. Briefly, live cells were resuspended in Annexin V binding buffer (10 mM Hepes pH 7.4, 140 mM NaCl, 2.5 mM $CaCl_2$) containing allophycocyanin (APC)-labeled Annexin V (BD Biosciences) and 7-amino-actinomycin D (7-AAD) as viability probe. A FACSCantoII flow cytometer, running with FACSDiVa software, was used for sample acquisition and analysis.

3. Results

3.1. SIL1 silencing activates PERK signalling and sensitizes HeLa cells to tunicamycin-induced ER stress

Approximately 60% of MSS cases are linked to homozygous or compound heterozygous *SIL1* mutations that make the SIL1 protein metabolically unstable, eventually leading to its loss [3,4]. To investigate the consequences of loss of SIL1 in a tractable cell model, we knocked down SIL1 expression in HeLa cells using three small interfering (si) RNAs (S2, S3 and S20). Western blot analysis showed that SIL1 expression was reduced by each of the three targeting siRNAs (Supplemental Fig. S2A), with > 80% reduction of SIL1 levels after 48–72 h, compared to cells transfected with two non-targeting siRNAs

(Supplemental Fig. S2B).

Western blot analysis found no significant increases in BiP, PDI and HSP47 protein levels in SIL1 KD cells compared to controls (Supplemental Fig. S3A and B). Quantitative reverse transcription PCR (RT-qPCR) showed only modest, non-significant up-regulation of sXBP1, ATF4 and BiP mRNAs (Supplemental Fig. S3C, white bars). However, there was a clear increase in eIF2α-P, and in the percentage of cells showing nuclear CHOP localization, indicating activation of PERK signalling (Supplemental Fig. S3A, B and D). Similar to what was observed in PCs and skeletal muscle fibres of woozy mice [19,20], ORP150 was higher in SIL1 KD than in control HeLa cells, most likely reflecting physiological up-regulation of this alternative BiP co-factor in response to diminished SIL1 activity (Supplemental Fig. S3A and B). Tunicamycin, a glycosylation inhibitor that induces ER stress by perturbing the folding efficiency in the ER, up-regulated sXBP1, ATF4 and BiP mRNAs in both control and SIL1 KD cells, but significantly more in the latter (Supplemental Fig. S3C; grey and black bars), indicating that loss of SIL1 sensitised cells to tunicamycin-induced ER stress.

3.2. SIL1 knock-down HeLa cells show chaperone aggregation in the ER, morphological alterations of the Golgi, autophagic vacuoles and mitochondrial enlargement

Loss of SIL1 function is expected to alter BiP-assisted folding in the ER, with potential deleterious effects on the homeostasis of the ER, and possibly other compartments of the secretory pathway which require a continuous supply of luminal or transmembrane proteins synthesized in the ER for their normal activity.

As a first approach to assess the consequences of SIL1 knockdown on the secretory pathway, we examined selected protein markers of different transport organelles by immunofluorescence confocal microscopy. Consistent with an impairment of the ER folding system, we found marked alterations in ER chaperone distribution, with calreticulin and HSP47 forming large perinuclear foci in SIL1 KD cells (Fig. 1A–F). Similar aggregates were observed for BiP and other ER-resident proteins such as PDI (Supplemental Fig. S4A and D). There was no difference between control and SIL1 KD cells in the distribution of Sec31, an essential component of the COPII coatomer complex, indicating no alterations in the ER exit sites (Supplemental Fig. S5A).

To assess the organization of the ER-Golgi intermediate compartment (ERGIC), we examined the distribution of ERGIC-53, an integral membrane protein that cycles between the ERGIC and the ER, and between the ERGIC and the cis Golgi [31]. In control cells ERGIC53 was mainly found in the perinuclear area, as expected, while in SIL1 KD cells it was abnormally concentrated in the Golgi region (Fig. 1G–I), suggesting perturbed transport between the ERGIC and Golgi [32].

Immunofluorescence staining of the cis and trans Golgi resident proteins GM130 and golgin-97 indicated marked alterations of the Golgi morphology in SIL1 KD HeLa cells (Fig. 1J–O). These markers were abnormally widespread throughout the cytoplasm of SIL1 KD cells (panels K and N), while cells transfected with the non-targeting siRNAs showed a typical distribution around the centrosome (panels J and M). Quantitative analysis of GM130 and golgin-97 dispersion along the x- and y-axes of the cells indicated that the Golgi was ~2.5 times more extended in SIL1 KD than in control cells (Fig. 1S and T).

Finally, we examined the endolysosomal compartment using antibodies against RAB5 to mark early endosomes, and LAMP1 to mark late endosomes/lysosomes. There was no significant difference in early endosome distribution between control and SIL1 KD HeLa cells (Supplemental Fig. S5B). In SIL1 KD cells, LAMP1-immunopositive vesicles were concentrated in large perinuclear clusters, whereas in control cells they were more widespread in the cytoplasm (Fig. 1P–R). Consistent with this, electron microscopy (EM) examination detected large clusters of autophagic vacuoles containing membranes and various electron-dense material (Fig. 2, compare panels A and D; and Table 1), reminiscent of the autophagic vacuoles seen in PCs and skeletal muscle fibres of MSS patients and woozy mice [18–20,24]. SIL1 KD cells had wider cis (the cisternae facing the nuclear membrane) and trans Golgi cisternae, but their number was not changed (Fig. 2C and F, yellow label; and Table 1). Finally, morphometric analysis of mitochondria indicated that their number per area was not changed but their average size was significantly greater (Fig. 2, compare panels B and E; and Table 1).

3.3. VSVG transport is delayed in SIL1 knockdown HeLa cells

To test whether the morphological alterations of secretory organelles were associated with impaired secretory protein transport, we used the temperature-sensitive vesicular stomatitis virus G protein (VSVG) cargo reporter. VSVG is a transmembrane glycoprotein widely used to monitor protein folding in the ER and the efficiency of the cell's transport machinery [29]. At 40 °C VSVG does not fold, and its exit from the ER is impaired. When cells are shifted to 32 °C, VSVG folds, exits the ER, and is synchronously transported through the secretory pathway. Control and SIL1 KD cells were infected with VSV, incubated at 40 °C for 3 h, then at 32 °C for 30 or 60 min in the presence of cycloheximide to prevent new protein synthesis, before fixation and immunofluorescence staining with antibodies against VSVG and GM130. After the 3-h incubation at 40 °C VSVG had a typical reticular distribution in both SIL1 KD and control cells, in-line with the expected impairment in its folding and accumulation in the ER (Fig. 3A, T_0). The pattern was markedly different 30 min after the temperature-block release, with almost all VSVG co-localizing with GM130 in control cells, while still largely in the ER in SIL1 KD cells (Fig. 3A and B, T_{30}), indicative of delayed VSVG folding and/or transport to the Golgi. After 60 min, VSVG had reached the plasma membrane (PM) in control cells, but still lagged in the Golgi in SIL1-KD cells (Fig. 3A and B, T_{60}).

3.4. Procollagen I and Na^+/K^+-ATPase accumulate intracellularly in SIL1 knockdown HeLa cells

The evidence that secretory trafficking of VSVG was delayed in SIL1 KD cells prompted us to check whether the transport of physiological cargoes was impaired. First, we recorded the cellular distribution of collagen I, which is a vital constituent of muscle tissue and important in PC migration, polarization and synaptogenesis [33]. Collagen I is synthesized as procollagen I (PC-I) in the ER, where it is folded and assembled in triple helices with the contribution of HSP47 before being transported through the secretory pathway and secreted in the extracellular space. Immunofluorescence analysis detected intracellular PC-I in ~10% of control HeLa cells. In SIL1 KD cultures the percentage was significantly higher: ~35%, with PC-I often forming large aggregates, ranging from 2 to 5 μm, which co-localized with HSP47 and BiP (Fig. 3C and D and Supplemental Fig. S4A–D). In some SIL1 KD cells a fraction of PC-I also co-localized with the Golgi complex, as shown by co-immunostaining with TGN46 (Supplemental Fig. S4E).

Next, we investigated the cellular distribution of Na^+/K^+-ATPase, whose pumping activity is vital for excitable cells like muscle fibres and neurons. In control HeLa cells, Na^+/K^+-ATPase showed the expected localization on the plasma membrane (PM); in contrast, in SIL1 KD cells Na^+/K^+-ATPase was less expressed on the cell surface and accumulated intracellularly, co-localizing largely with the Golgi marker GM130 (Fig. 4). We also studied this abnormal localization by immunofluorescence analysis after treatment with nocodazole, a microtubule polymerization inhibitor that causes fragmentation of the Golgi ribbon into isolated stacks of cisternae, facilitating cargo visualization. In nocodazole-treated SIL1 KD cells, Na^+/K^+-ATPase appeared as discrete spots co-localized with GM130 and TGN46 (Supplemental Fig. S6), confirming its accumulation in the Golgi.

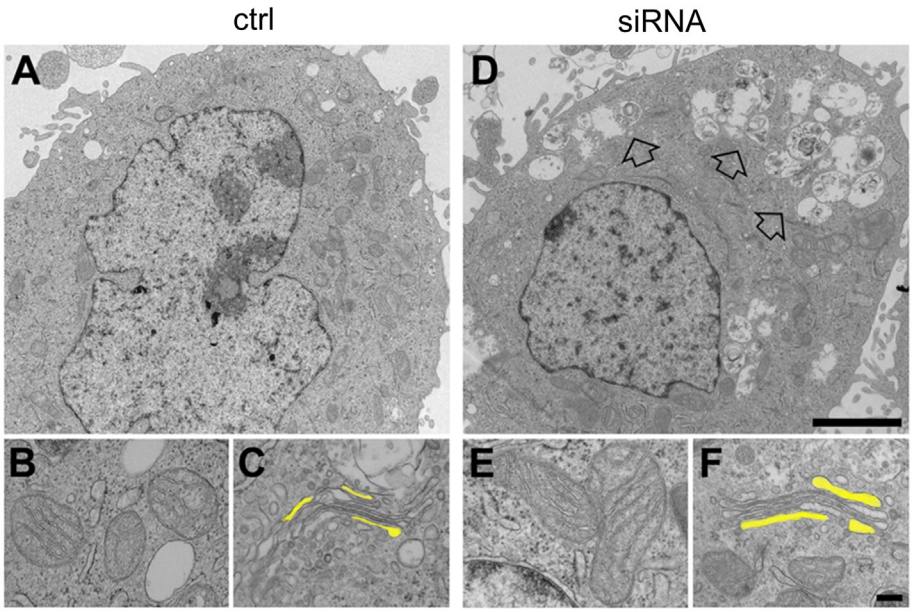

Fig. 2. Ultrastructural alterations in SIL1 KD HeLa cells. (A–C) Representative EM micrograph of a control HeLa cell (A). Details at higher magnification of mitochondria (B) and a Golgi apparatus (C). (D–F) Representative EM micrograph of a SIL1 KD (S2) HeLa cell: arrows point to groups of vacuoles containing membranes or other electron-dense material. Details at higher magnification of mitochondria (E) and a Golgi apparatus (F). Yellow in panels C and F labels the nuclear and apical cisternae of the Golgi. Scale bars: 2 μm (A and D); 0.2 μm (B, C, E and F).

3.5. The rate of apoptosis is increased in SIL1 knockdown HeLa cells

To see whether SIL1 silencing had any effect on the viability of HeLa cells, as a first approach, we counted the number of cells in control and SIL1 KD cultures 72 h after siRNA transfection: SIL1-interfered cells were ~43% less than cells transfected with the control siRNAs. To determine whether this difference was due to an increase in the rate of cell death or reduced cell proliferation, we used trypan blue, which selectively stains dead cells. Trypan blue-positive cells in SIL1 KD cultures double that in controls (33 ± 2.8% vs. 14 ± 2.3%; mean ± SEM, n = 3; $p < 0.01$ by Student's *t*-test). This was confirmed by laser flow cytometry with the cell impermeant DNA dye 7-amino-actinomycin D (7-AAD), which showed an increase in 7-AAD-positive (i.e. death) cells (Fig. 5A), and by MTT assay, indicating a strong reduction in the metabolic activity of SIL1 KD cells compared to controls (Fig. 5B).

Several items of evidence indicated that cell death occurred by apoptosis. First, SIL1 KD cultures showed significantly higher percentages of cells with pyknotic nuclei and fragmented DNA, detected by Hoechst 33342 staining and TUNEL assay, respectively (Fig. 5C and D). Second, there was an increase in cells positive for annexin V, indicative of cell surface exposure of phosphatidylserine, which marks apoptotic cells for phagocytosis (Fig. 5A and E). Finally, analysis of DNA content by propidium iodide-flow cytometry showed a larger number of cells in the sub-G1 phase, indicative of apoptosis, in SIL1 KD than in control cultures (Figs. 5F and 8B), but no differences in the proportions of cells in the G1, S and G2 phases of the cell cycle (Supplemental Fig. S7). Thus, SIL1 silencing increased HeLa cell apoptosis, with no detectable effect on their proliferation rate.

To investigate the molecular pathways activated by loss of SIL1, we analysed the expression of 84 genes involved in cell death (Cell Death Pathway Finder, RT2 Profiler PCR Array, Qiagen). We found significant increases in the expression of both apoptosis- and autophagy-related genes, the most relevant of which were ATG3, ATG5, APP, JNK1, ATP6V1G2, DENND4A, GALNT5 and NFKB1, and a significant down-regulation of TRAF2.

3.6. GSK2606414 treatment rescues the morphofunctional abnormalities of the secretory pathway and reduces apoptotic cell death induced by SIL1 knockdown

Previous studies have shown that pharmacological inhibition of the PERK pathway to restore protein synthesis during ER stress has marked protective effects in protein-misfolding neurodegenerative disease mouse models [34–37]. Since PERK signalling was activated in SIL1 KD HeLa cells, as shown by increased eIF2α-P and nuclear CHOP localization, we investigated whether PERK inhibition had any effect on the morphological and functional abnormalities of the secretory pathway, and cell viability.

HeLa cells were transfected with control or SIL1-targeting siRNAs, exposed to the potent PERK inhibitor GSK2606414 (250 nM) or vehicle 24 h after transfection, and analysed 48 h later. GSK2606414 significantly reduced the percentages of cells with HSP47 and calreticulin aggregates, and abnormal Golgi morphology, detected by golgin-97 staining (Fig. 5G–I). Ultrastructural analysis showed that the size of the cis and trans cisternae of the Golgi stack in GSK2606414-treated cells was the same as controls (Fig. 6A–D; and Table 1); the percentage of vacuolated cells was also significantly lower, and the size of

Table 1
Quantitative analysis of ultrastructural alterations in controls and SIL1 KD HeLa cells.

	Cells with accumulation of vacuoles, %	N° of Golgi stacks/100 μm^2	N° of cisternae/ stack	Cis cisterna width (nm)	Trans cisterna width (nm)	N° of mitochondria/ 100 μm^2	Mitochondria average size (μm^2 × 10^{-1})
Ctrl	12	2.7 ± 0.3	3.9 ± 0.1	25.1 ± 1.6	27.6 ± 2.0	22.9 ± 2.0	2.8 ± 0.01
Ctrl + GSK	17	2.3 ± 0.3	4.3 ± 0.2	25.9 ± 1.7	29.2 ± 3.1	25.5 ± 1.6	3.0 ± 0.2
SIL1 KD	61*	2.9 ± 0.5	4.0 ± 0.2	40.8 ± 4.6*	38.2 ± 3.2*	20.3 ± 1.9	4.1 ± 0.02*
SIL1 KD + GSK	27≠	2.3 ± 0.7	4.2 ± 0.2	30.9 ± 1.8≠	26.9 ± 1.5≠	20.8 ± 1.8	3.2 ± 0.01≠

Values are shown as mean ± SEM.
* $p < 0.05$ vs. Ctrl.
≠ $p < 0.05$ vs. SIL1 KD.

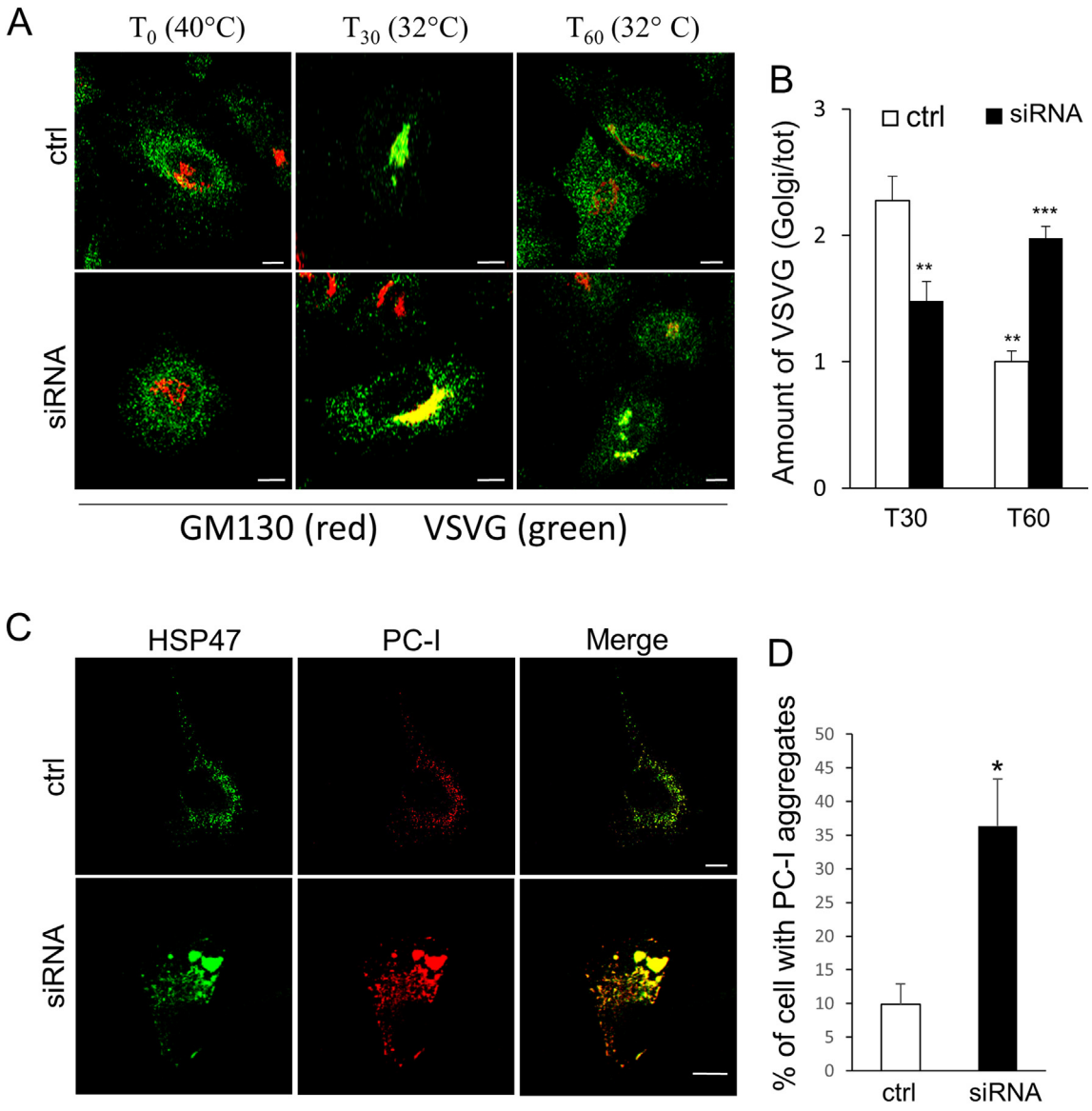

Fig. 3. Cargo transport is delayed in SIL1 KD HeLa cells. (A) HeLa cells were incubated with VSV at 32 °C for 45 min 72 h after transfection with ctrl or SIL1 (S20) siRNAs, then at 40 °C for 3 h (temperature block) and at 32 °C for the indicated times (temperature-block release) in the presence of cycloheximide. Cells were fixed and stained for VSVG (green) and GM130 (marker for Golgi area definition, red). Scale bars, 10 μm. (B) The bar graph shows the mean ratio ± SEM of the amount of VSVG in the Golgi to the total VSVG of three independent experiments. Ctrl and siRNA are represented by white and black bars respectively. **$p < 0.01$ vs. control at T_{30}; ***$p < 0.001$ vs. ctrl at T_{60} by Student's *t*-test. (C) HeLa cells transfected with ctrl or SIL1 (S2) siRNAs were fixed after 72 h and stained for PC-I (red) and HSP47 (green) as indicated. Merged images of red and green signals are shown. Scale bars, 10 μm. (D) The graph shows the percentages of cells containing intracellular accumulation of PC-I. Data are the mean ± SEM of three independent experiments. *$p < 0.05$ vs. control by Student's *t*-test.

mitochondria was comparable to that of non-interfered cells (Fig. 6E–H; and Table 1). The percentage of SIL1 KD cells with PC-I aggregates in the ER was also significantly reduced by the inhibitor (Fig. 7A and B). Western blot analysis showed a small increase in the amount of intracellular PC-I in SIL1 interfered cells, and this was not rescued by GSK2606414 treatment (Fig. 7C). Thus, GSK2606414 treatment reduced the number of cells with PC-I aggregates, consistent with its positive effect on chaperone aggregation, but had no effect on the increase in PC-I seen by Western blot, perhaps because of restored PC-I synthesis upon PERK inhibition.

GSK2606414 significantly improved survival of SIL1 KD HeLa cells. Hoechst 33342 staining showed fewer cells with pyknotic nuclei compared to vehicle-treated SIL1 KD controls (Fig. 8A). DNA content and annexin V staining measured by flow cytometry confirmed the protective effect of GSK2606414 on apoptotic cell death (Fig. 8B and C).

3.7. SIL1 knockdown alters ER homeostasis and secretory transport, and reduces the viability of SH-SY5Y cells

To test whether the effects of siRNA-mediated SIL1 silencing documented in HeLa cells held true in other cell types, we knocked down SIL1 expression in SH-SY5Y neuroblastoma cells. Like in HeLa cells, there was no full UPR activation in the silenced SH-SY5Y cells, but their response to tunicamycin was boosted, as shown by their significantly higher levels of sXBP1, ATF4 and BiP mRNAs compared to tunicamycin-treated SIL1-expressing cells (Supplemental Fig. S8B). Calreticulin and HSP47 were aggregated in SIL1-interfered SH-SY5Y cells (Fig. 9). Specifically, while the percentages of control cells showing calreticulin and HSP47 aggregates were 3 and 8.6% respectively, these percentages were 23 and 52% in interfered cells. After treatment with GSK2606414 the percentages of cells showing calreticulin and HSP47 aggregates did not change in controls but were

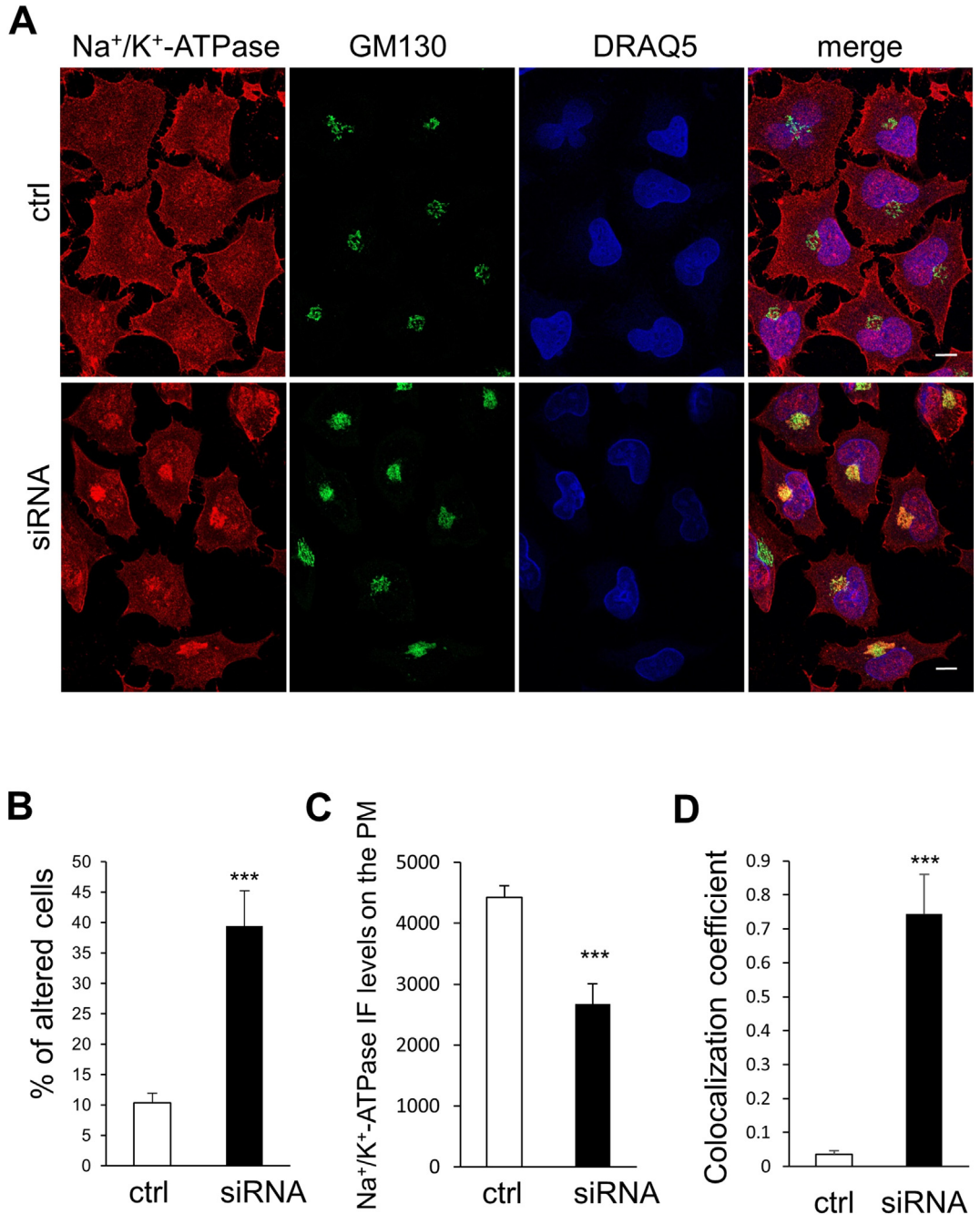

Fig. 4. Golgi accumulation of Na^+/K^+-ATPase alpha1 in SIL1 KD HeLa cells. (A) HeLa cells transfected with ctrl or SIL1 (S20) siRNAs were fixed after 72 h and stained with anti-Na^+/K^+-ATPase alpha1 (red) and anti-GM130 (green) antibodies and with DRAQ5 (blue) to identify the nuclei. Merged images of blue, red and green signals are also shown. Scale bars, 10 μm. (B–C) The graphs shows the percentages of cells with an accumulation of Na^+/K^+-ATPase alpha1 at the Golgi (B) and the amount of Na^+/K^+-ATPase alpha1 fluorescence at the plasma membrane, PM (C). (D) Quantification of the colocalization between the Na^+/K^+-ATPase and the Golgi marker GM130. Data are the mean ± SEM of three independent experiments. ***$p < 0.001$ vs. control by Student's *t*-test.

significantly reduced in SIL1-interefered cells to 4.7 and 9.8%.

Immunostaining of the secretory cargo PC-I showed intracellular patches, not colocalizing with ER markers, in about 53% of the SIL1 KD cells, whereas these structures were present only in 7% of control cells (Fig. 10, arrowheads). Furthermore, PC-I accumulated in the Golgi complex of 12% of interfered cells and 1% of control cells (Fig. 10). GSK2606414 treatment did not improve PC-I transport in SIL1 KD cells (Fig. 10). Ultrastructural analysis showed large vacuoles in the majority of SIL1 KD SH-SY5Y cells, which were seen only in few control cells, whereas the number of Golgi stacks, the width of the Golgi cisternae and the average size of mitochondria were similar (Fig. 11A and C). GSK2606414 treatment reduced the number of cells with vacuole accumulation (Fig. 11C and D). Finally, apoptotic cell death was significantly increased in SIL1 interfered SH-SY5Y cells compared to controls (Supplemental Fig. S8C and D).

4. Discussion

In the present study, siRNA-mediated knockdown of SIL1 in HeLa cells induced marked morphological and functional changes in the secretory pathway, with protein aggregation and retention in the ER and Golgi. SIL1 KD cells also had accumulation of autophagic vacuoles,

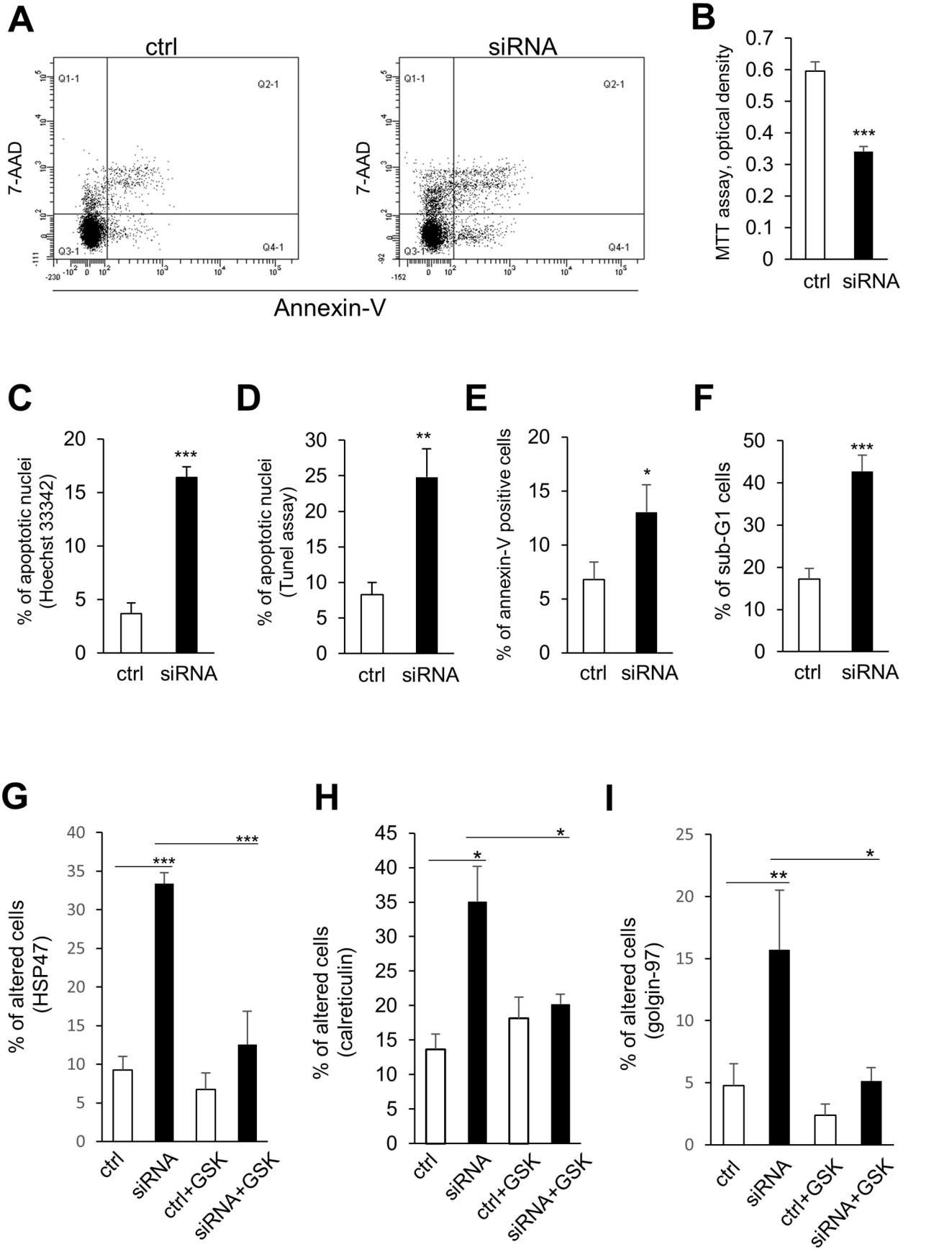

(caption on next page)

Fig. 5. SIL1 knockdown induces apoptotic cell death. HeLa cells were transfected with control (ctrl) or SIL1 (S2) siRNAs, and the total, live or apoptotic cells were quantified after 72 h by: (A) 7–amino–actinomycin D (7-AAD) vital staining; (B) MTT proliferation assay; (C) Hoechst 33342 staining; (D) TUNEL assay; (B–E) annexin V staining; and (F) propidium iodide staining. (G–I) HeLa cells were transfected with ctrl or SIL1 (S2) siRNAs and treated with vehicle or GSK2606414 (250 nM) in Opti-MEM after 24 h, and the percentages of cells with HSP47 and calreticulin aggregates or altered of Golgi morphology were recorded 48 h later. Data are means ± SEM of three independent experiments; ***p < 0.001, **p < 0.01, *p < 0.05 by Student's *t*-test.

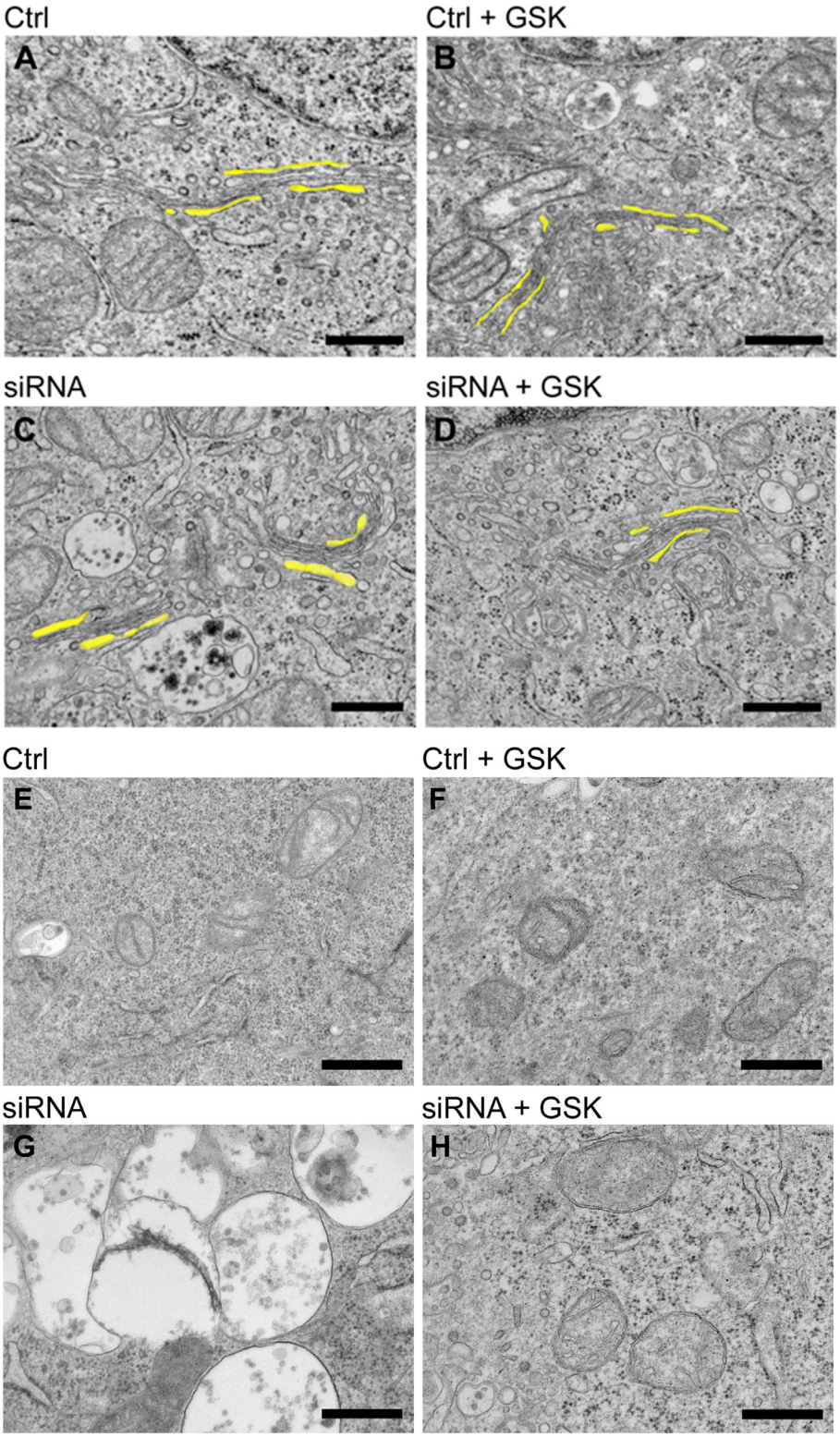

Fig. 6. GSK2606414 improves cell morphology in SIL1 KD HeLa cells. (A–H) Representative EM micrographs of HeLa cells transfected with SIL1 (S2) siRNAs, treated with vehicle (A, C, E and G) or GSK2606414 (250 nM) in Opti-MEM after 24 h and analysed 48 h later (B, D, F and H). The cis and trans Golgi cisternae are labeled yellow (A–D). Vacuoles accumulation are shown in panel E–H. Data are representative of two independent experiments. Scale bars 0.5 μm.

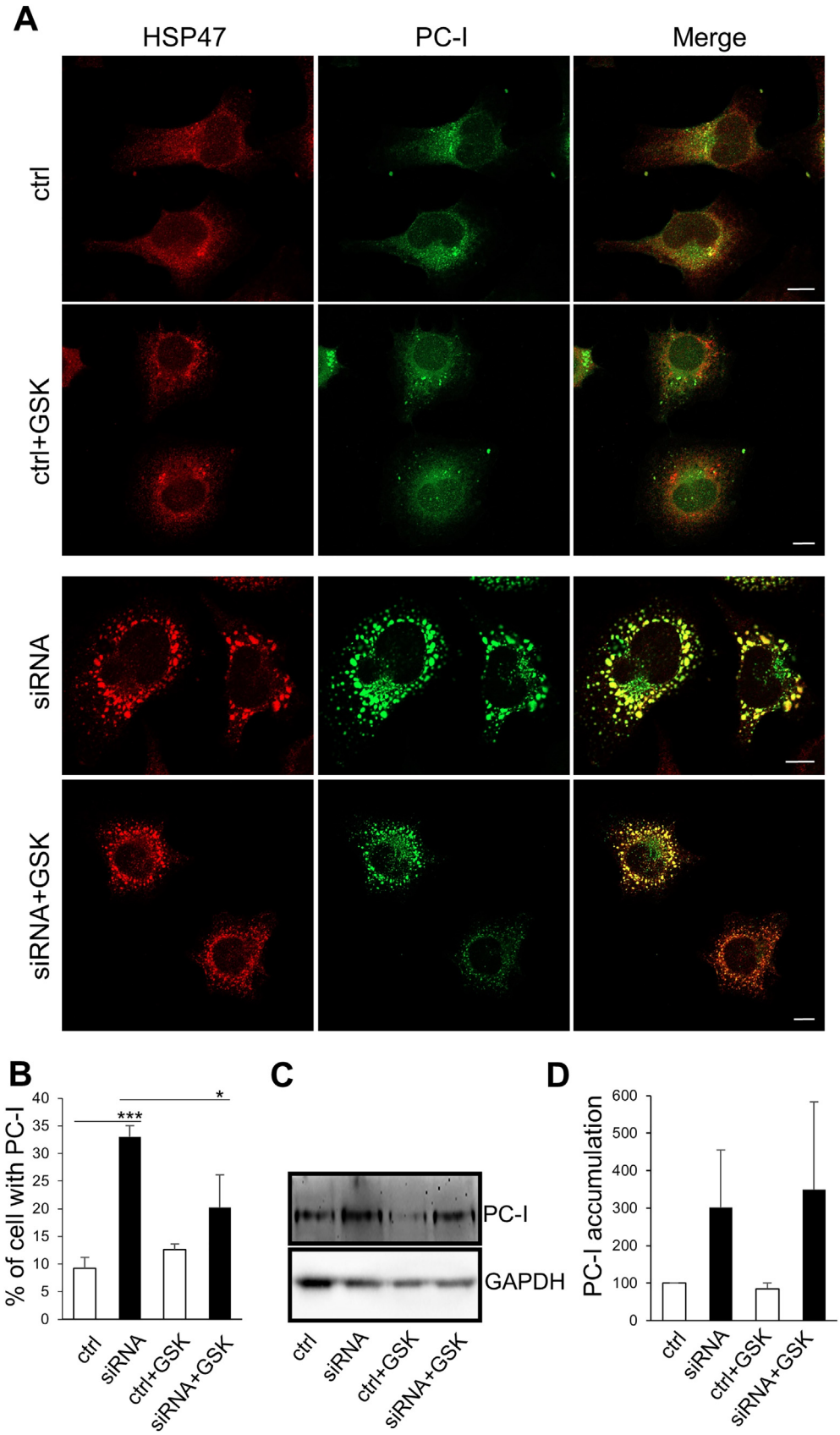

Fig. 7. GSK2606414 improves the transport of PC-I in SIL1 KD HeLa cells. (A) HeLa cells transfected with control (ctrl) or SIL1 siRNAs (S2) were treated with the vehicle or GSK2606414 (250 nM) in Opti-MEM 24 h after transfection and fixed and stained for PC-I (red) and HSP47 (green) after 48 h. Scale bars, 10 μm. (B) Percentages of cells with accumulation of intracellular PC-I. Data are the mean ± SEM of three independent experiments. ***$p < 0.001$ vs. control; *$p < 0.05$ vs. siRNA by Student's *t*-test. (C) HeLa cells treated as in A, were lysed and PC-I revealed by Western blotting. GAPDH is shown as loading control. (D) Quantification of two independent experiments as shown in C.

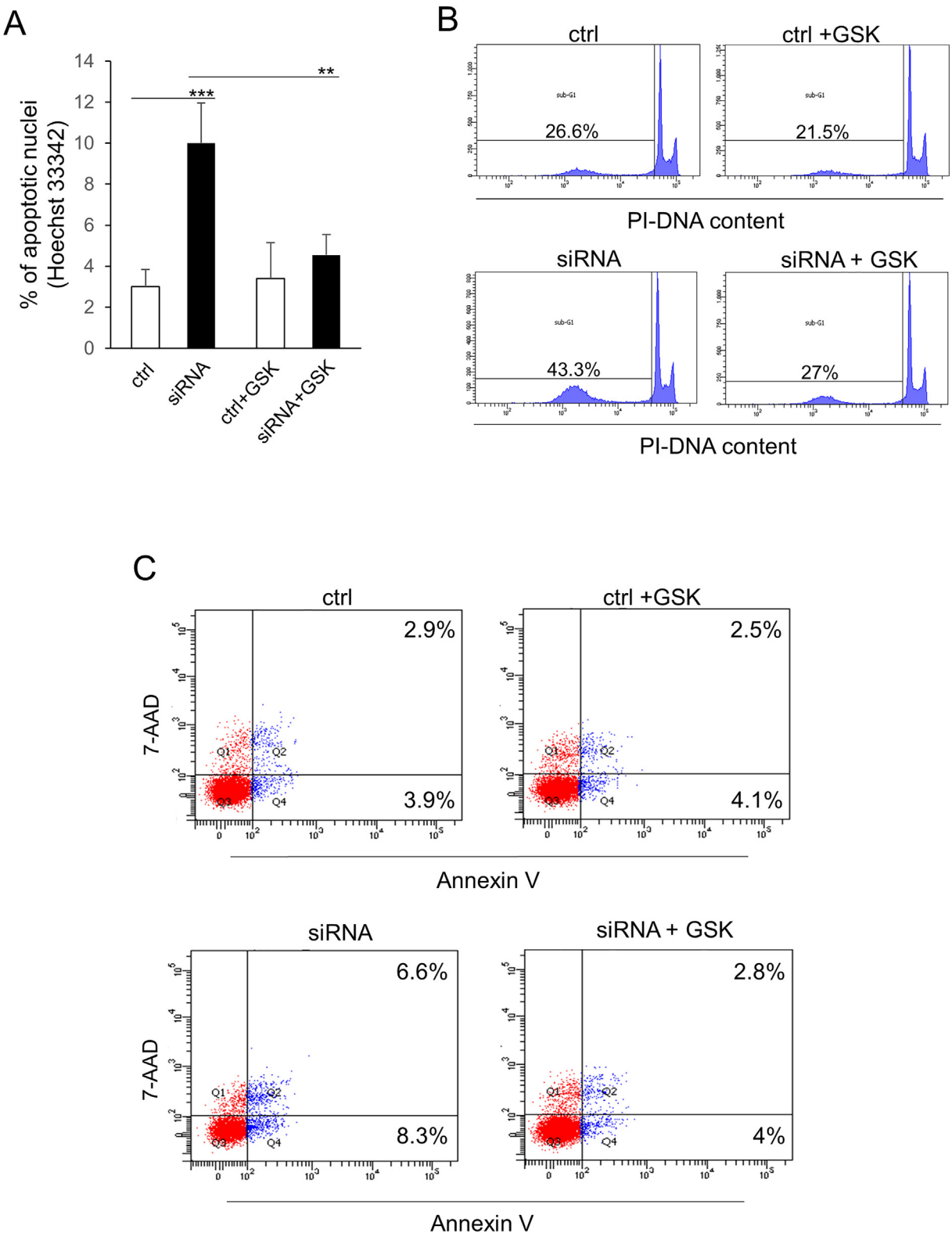

Fig. 8. GSK2606414 reduces the apoptosis in SIL1 KD HeLa cells. (A–C) HeLa cells were transfected with ctrl or SIL1 siRNAs (S20) and treated with vehicle or GSK2606414 (250 nM) in Opti-MEM after 24 h, and apoptosis was determined 48 h later by (A) Hoechst 33342, (B) propidium iodide (PI) and Annexin V staining (C). The scatter plots show the distribution of 7-AAD-positive and annexin V-negative (Q1), 7-AAD- and annexin V-positive (Q2), 7-AAD-negative and annexin V-positive (Q4) and 7-AAD- and annexin V-negative (Q3) cells. The percentages of apoptotic cells in Q2 and Q4 are indicated. Data in A are means ± SEM of three independent experiments. ***$p < 0.001$ vs. controls; **$p < 0.01$ vs siRNA by Student's *t*-test. Data in B and C are representative of three independent experiments.

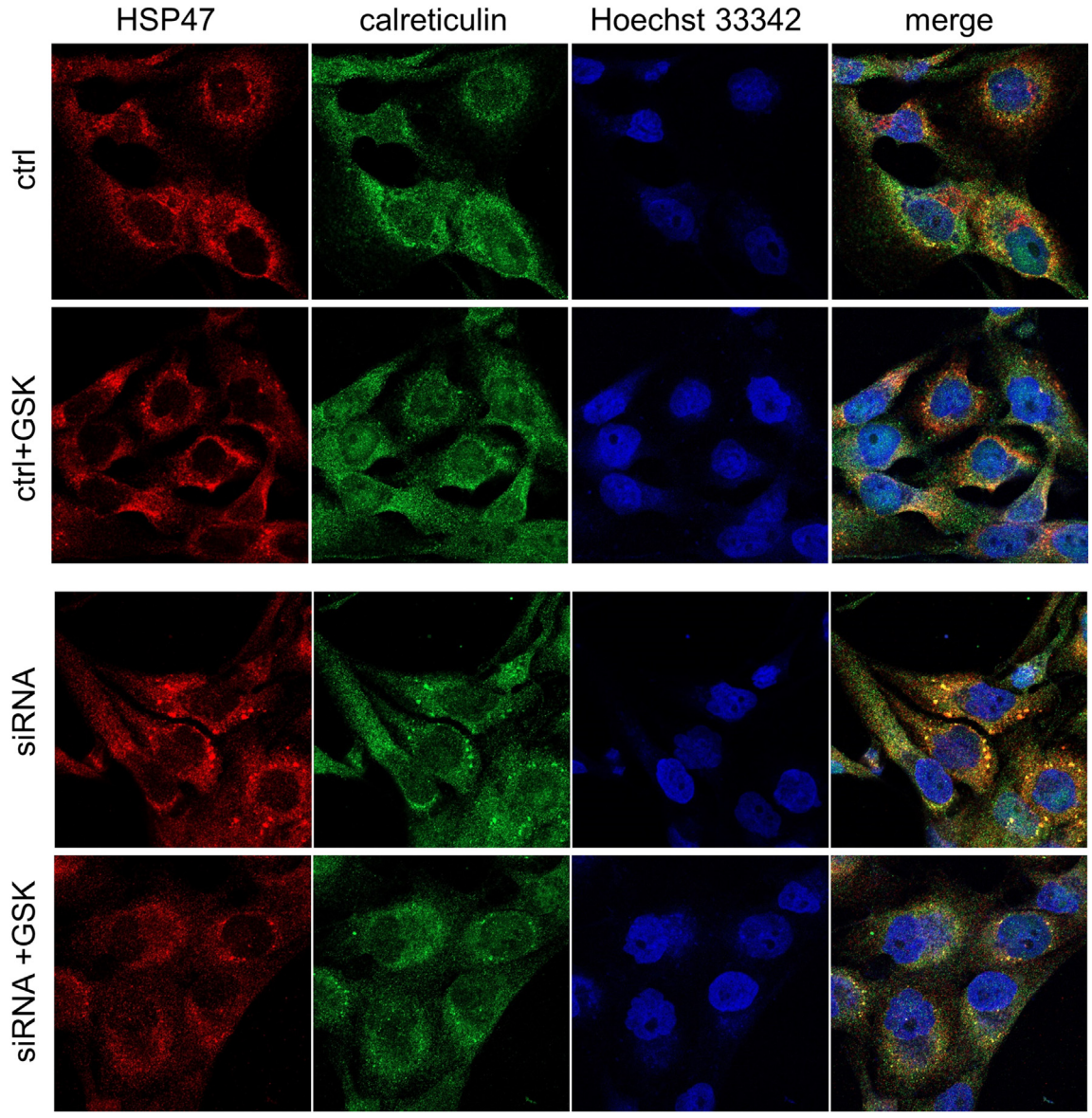

Fig. 9. GSK2606414 treatment reduces chaperone aggregates triggered by SIL1 knock down in SH-SY5Y. SH-SY5Y cells were transfected with ctrl or SIL1 (S3) siRNAs and treated with vehicle or GSK2606414 (500 nM) in complete medium 48 h after transfection. The cells were stained for HSP47 (red) and calreticulin (green) in combination with Hoechst 33342 (blue) 24 h later. Scale bars, 10 μm. Data are representative of two independent experiments.

enlarged mitochondria, and an increased rate of apoptosis. The PERK branch of the UPR was activated, and pharmacological inhibition of PERK attenuated the morphofunctional abnormalities of the secretory pathway and significantly reduced apoptosis. These findings indicate that SIL1 deficiency alters secretory transport, potentially contributing to the cellular pathology of MSS. They call for further investigations to assess the role of impaired intracellular protein transport in selective vulnerability, and to test the therapeutic potential of PERK signalling inhibition.

We found that silencing SIL1 expression induced several molecular and morphological alterations in HeLa cells, some of them reminiscent of those described in degenerating tissues of MSS patients and woozy mice [19,24–27]. Like in woozy PCs and skeletal muscle fibres, ORP150 was up-regulated in SIL1 KD HeLa, and there were rises in the eIF2α-P level and in the number of CHOP-positive nuclei, indicating PERK branch activation. Other UPR markers were only modestly up-regulated by SIL1 knockdown, but cells were significantly more prone to tunicamycin-induced ER stress, consistent with impaired BiP-assisted protein folding in the ER, and with the observation that loss of one functional *SIL1* allele makes motor neurons more vulnerable to mutant SOD1-induced ER stress [38].

Immunofluorescence analysis showed that several molecular chaperones, including calreticulin, HSP47, PDI and BiP, were present in large foci in the ER lumen, and BiP, PDI and HSP47 co-localized with aggregated PC-I, suggesting an attempt to counteract protein aggregation.

SIL1 KD HeLa cells also had abnormal distributions of ERGIC, Golgi and lysosome markers, indicating that the effects of SIL1 silencing extended beyond the ER. ERGIC53 was abnormally concentrated in the Golgi region, GM130 and golgin-97, which mark the cis and trans Golgi respectively, were more widespread in the cytoplasm, and LAMP1 had an abnormal perinuclear distribution, indicating important morphological alterations of post-ER compartments of the secretory pathway and increased lysosomal activity. In line with this, ultrastructural analysis indicated an enlargement of the Golgi cisternae and increased autophagic vacuoles. It also documented mitochondrial swelling, perhaps indicative of the ongoing apoptotic process (see below). Diffuse cell vacuolation and abnormal mitochondria have been reported in PCs and

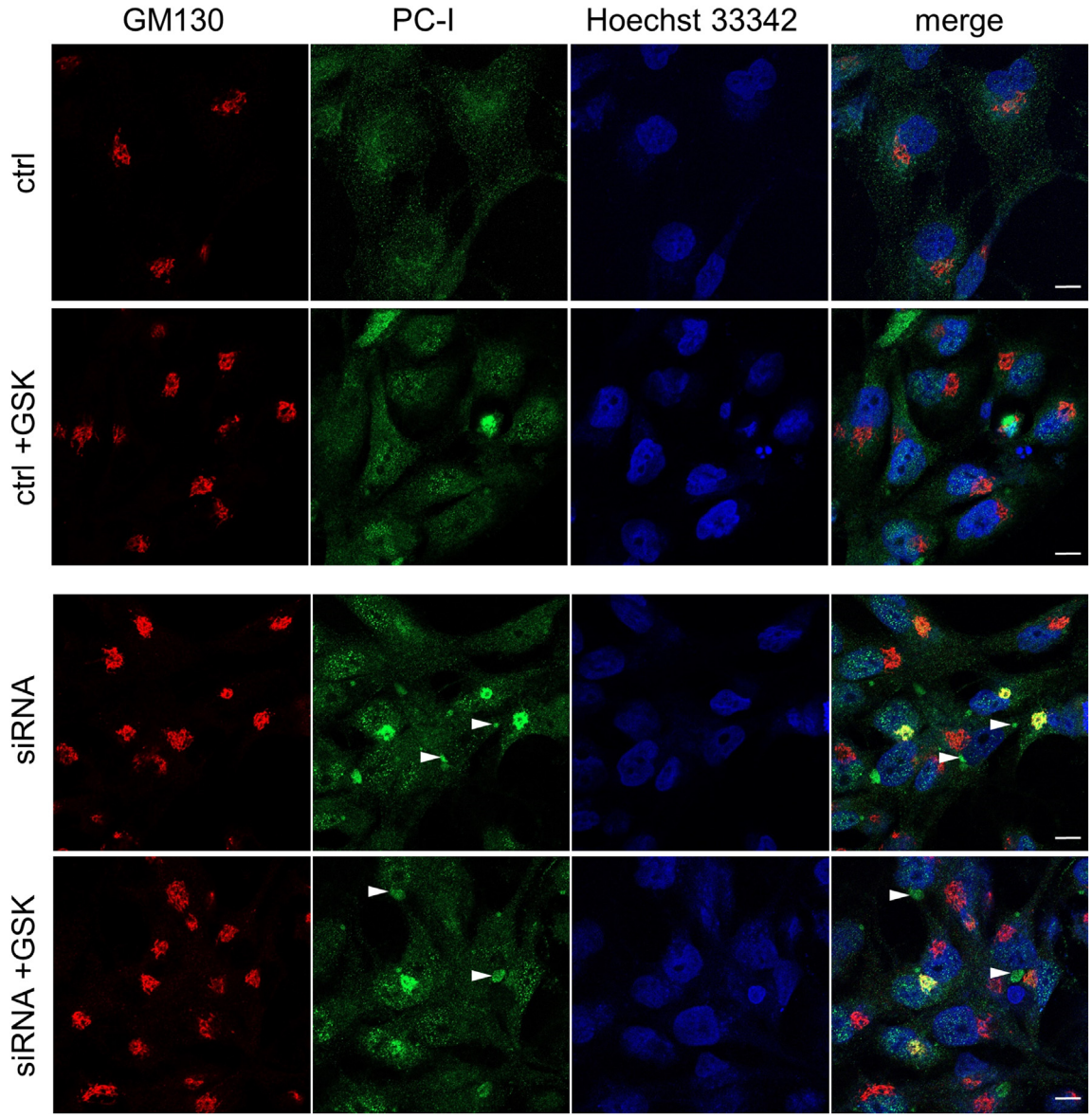

Fig. 10. GSK2606414 treatment reduces chaperone aggregates triggered by SIL1 knock down in SH-SY5Y. SH-SY5Y cells were transfected with ctrl or SIL1 (S3) siRNAs and treated with vehicle or GSK2606414 (500 nM) in complete medium 48 h after transfection. The cells were stained for GM130 (red) and PC-I (green) in combination with Hoechst 33342 (blue) 24 h later. Scale bars, 10 μm. Data are representative of two independent experiments.

skeletal muscle fibres of MSS patients and woozy mice [19,20,24–27]. Thus, SIL1 KD HeLa cells recapitulated key features of the in vivo pathology with the exception of the nuclear envelope alterations.

Interestingly gene expression analysis of SIL1 KD HeLa cells identified an increase in JNK1, a stress factor activated kinase that is engaged by the UPR and is involved in both autophagy and apoptosis [15,16]. TNF signalling also appeared to be engaged, considering that NFKB1 was upregulated and TRAF2 downregulated. A previous study demonstrated that IRE1-mediated activation of NFKB1 is required for UPR-induced cell death, while TRAF2 is downregulated during ER stress, and this promotes TNF-induced apoptosis [39].

We found that the morphological changes of the secretory pathway were associated with defective secretory transport of the VSVG cargo reporter. At the end of the 40 °C incubation step, the amount of VSVG in the Golgi was negligible in both control and SIL1 KD cells, with most VSVG molecules retained in the ER as a result of temperature-induced misfolding. In line with our previous analysis [40], the amount of VSVG in the Golgi of control cells increased with incubation at 32 °C, reaching a peak after 30 min (T30), then decreased as the protein was transported out of the Golgi, reaching the PM at 60 min (T_{60}). Compared to controls, at T_{30} less VSVG had exited the ER and reached the Golgi in SIL1 KD HeLa, indicating impaired protein folding in the ER or lower efficiency of ER-to-Golgi transport, or both.

Interestingly, in SIL1 KD cells there was more VSVG in the Golgi complex at T_{60} than at T_{30}. This may result from delayed en-bloc folding of VSVG molecules in the ER and their synchronous transport to the Golgi, or from diminished Golgi to PM transport. A Golgi dysfunction is suggested by ultrastructural analysis, with swelling of the first and last cisternae of the stacks. Moreover, immunofluorescence analysis of SIL1 KD HeLa cells showed massive Na^+/K^+-ATPase accumulation in the Golgi complex. Finally, PC-I, a protein whose folding, assembly and secretory transport is particularly demanding for the cell, accumulated in both the ER and Golgi of SIL1 interfered cells, supporting both reduced ER folding capacity and impaired cargo transport beyond the Golgi.

SIL1 knockdown in SH-SY5Y and HeLa cells had similar effects. Compared to controls, SIL1 KD SH-SY5Y cells showed chaperone aggregates in the ER, altered PC-I transport, cytoplasmic vacuoles, and a

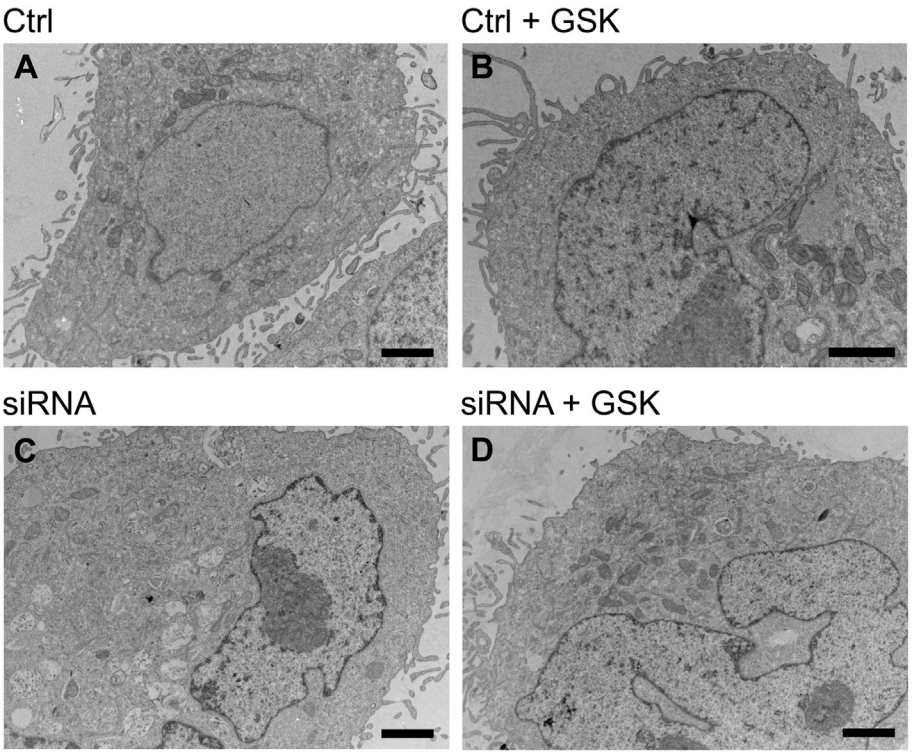

Fig. 11. GSK2606414 improves cell morphology in SH-SY5Y KD HeLa cells. (A–D) Representative EM micrographs of SH-SY5Y cells transfected with SIL1 (S20) siRNA, treated with vehicle (A and C) or GSK2606414 (250 nM) in Opti-MEM after 24 h and analysed 48 h later (B and D). Data are representative of two independent experiments. Scale bars 0.5 μm.

higher rate of apoptosis. They were also more prone to tunicamycin-induced ER stress than controls. These phenotypes, however, were less marked than in HeLa cells, and in some cases slightly different. For example, PC-I aggregated mainly in the ER in SIL1-interfered HeLa cells with only a minor fraction in the Golgi, whereas it was mostly in the Golgi in SH-SY5Y interfered cells. It remains to be established whether these differences reflect cell-specific responses to SIL1 knockdown or are due to slight differences in the efficiency of SIL1 interference.

We also detected alterations in secretory trafficking and higher apoptotic rates in HeLa and SH-SY5Y cells in which SIL1 was chronically silenced by transduction with lentivirus encoding anti-SIL1 short-hairpin RNAs (Supplemental Fig. S9). These effects, however, were much less evident than after acute siRNA-mediated knockdown despite similar down-regulation of SIL1, indicating that cells adapt to loss of SIL1. We also found no alterations in Na^+/K^+-ATPase distribution, CHOP activation or increased apoptotic rate in mouse embryonic fibroblasts from woozy mice maintained in culture for several weeks (Supplemental Fig. S10). Therefore, SIL1, although expressed ubiquitously, appears to be dispensable for many cell types upon adaptation. In some cells, however, adaptation mechanisms seem inadequate and eventually lead to cell death. Interestingly, genetic deletion of neuronal GM130 in mice caused Golgi fragmentation and impaired secretory trafficking in Purkinje neurons, resulting in apoptotic cell death and ataxia [41], supporting the view that alterations in secretory trafficking induced by loss of SIL1 may contribute to selective PC degeneration in MSS. In other cells, SIL1 loss might cause milder phenotypes. For example, pyramidal cortical neurons of woozy mice migrate more slowly than wild-type cells during neurodevelopment, but they eventually reach their final destination [42].

Our findings that SIL1 silencing alters secretory transport suggest SIL1 mutations may selectively affect cells that require optimal secretory capacity for their function, such as Purkinje neurons and skeletal muscle cells, which may be particularly dependent on efficient PM delivery of ion channels, neurotransmitter and/or trophic factor receptors. In this study we started analysing the trafficking of cargoes potentially important for these cells using the SIL1 KD HeLa model, and found impaired PM expression of the Na^+/K^+-ATPase pump and secretion of collagen. It will now be important to carry out similar studies in primary PC and skeletal muscle cultures of woozy mice to identify other molecules whose disrupted transport may contribute to cell dysfunction and death. These studies will not only cast light on the physiopathology of MSS but may also help devise effective therapeutic approaches.

In this regard, we report here that the PERK branch of the UPR was particularly active in SIL1 KD HeLa cells, and the PERK inhibitor GSK2606414 unexpectedly reduced the morphofunctional abnormalities of the secretory pathway and significantly reduced apoptotic cell death. Interstingly, in SH-SY5Y cells transport was mainly impaired at the Golgi and it was not rescued by GSK2606414, consistent with PERK inhibition acting primarily on ER function.

Blocking PERK/eIF2α translational attenuation in mouse models of prion disease and frontotemporal dementia restored the synthesis of vital pre- and post-synaptic proteins, with positive effects on synaptic transmission, neuronal survival and behaviour [35,37,43]. It is tempting to speculate that recovery of protein synthesis might also explain the beneficial effects of GSK2606414 on trafficking in SIL1 KD HeLa cells, perhaps because it permits more efficient translation of ER chaperones and/or vital proteins of the cell transport machinery. Our results also raise the intriguing possibility that PERK signalling may govern secretory membrane trafficking. However, PERK is involved in controlling autophagosome formation and mitochondrial proteostasis [44,45], and inhibition of these activities may have contributed to the beneficial effects in HeLa cells. Finally, we cannot exclude that off-target effects of the inhibitor may also have participated in rescuing cell death [46]. Whatever the mechanisms, our findings suggest that inhibition of PERK signalling may be a useful therapeutic strategy for MSS. Supporting this, we have recently found that inhibiting PERK signalling with GSK2606414 delays Purkinje cell death and ameliorates muscle pathology and motor performance in woozy mice [47].

Supplementary data to this article can be found online at https://doi.org/10.1016/j.bbadis.2018.07.003.

Conflict of interest

The authors declare that they have no conflicts of interest with the contents of this article.

Author contributions

C.V. performed cell transfections, confocal microscopy experiments and western blot analysis of UPR markers; E.C. performed flow cytometry and MTT experiments; E.R. contributed to cell transfections and western blot analysis of UPR markers; A.D.C. performed some confocal confocal microscopy experiments; S.S. performed biochemical experiments; F.O. carried out experiments in woozy mouse embryonic fibroblasts; L.P. performed EM experiments; F.P. supervised the EM experiments; R.C. and M.S. conceived and supervised the study, analysed the results, and wrote the manuscript.

Funding

This work was supported by the Italian Telethon ONLUS Foundation, Rome, Italy (grant N° GGP12220 to MS and RC and N° GGP13213 to FP).

Transparency document

The Transparency document associated with this article can be found, in online version.

References

[1] G. Marinescu, S. Draganesco, D. Vasiliu, Nouvelle maladie familiale caractérisée par une cataracte congénitale et un arret du développement somato—neuro-psychique, L'Encéphale 26 (1931) 97–109.
[2] T. Sjogren, Hereditary congenital spinocerebellar ataxia accompanied by congenital cataract and oligophrenia; a genetic and clinical investigation, Confin. Neurol. 10 (1950) 293–308.
[3] A.K. Anttonen, I. Mahjneh, R.H. Hamalainen, C. Lagier-Tourenne, O. Kopra, L. Waris, M. Anttonen, T. Joensuu, H. Kalimo, A. Paetau, L. Tranebjaerg, D. Chaigne, M. Koenig, O. Eeg-Olofsson, B. Udd, M. Somer, H. Somer, A.E. Lehesjoki, The gene disrupted in Marinesco-Sjogren syndrome encodes SIL1, an HSPA5 cochaperone, Nat. Genet. 37 (2005) 1309–1311.
[4] J. Senderek, M. Krieger, C. Stendel, C. Bergmann, M. Moser, N. Breitbach-Faller, S. Rudnik-Schoneborn, A. Blaschek, N.I. Wolf, I. Harting, K. North, J. Smith, F. Muntoni, M. Brockington, S. Quijano-Roy, F. Renault, R. Herrmann, L.M. Hendershot, J.M. Schroder, H. Lochmuller, H. Topaloglu, T. Voit, J. Weis, F. Ebinger, K. Zerres, Mutations in SIL1 cause Marinesco-Sjogren syndrome, a cerebellar ataxia with cataract and myopathy, Nat. Genet. 37 (2005) 1312–1314.
[5] K.T. Chung, Y. Shen, L.M. Hendershot, BAP, a mammalian BiP-associated protein, is a nucleotide exchange factor that regulates the ATPase activity of BiP, J. Biol. Chem. 277 (2002) 47557–47563.
[6] N.N. Alder, Y. Shen, J.L. Brodsky, L.M. Hendershot, A.E. Johnson, The molecular mechanisms underlying BiP-mediated gating of the Sec61 translocon of the endoplasmic reticulum, J. Cell Biol. 168 (2005) 389–399.
[7] N.G. Haigh, A.E. Johnson, A new role for BiP: closing the aqueous translocon pore during protein integration into the ER membrane, J. Cell Biol. 156 (2002) 261–270.
[8] P. Maattanen, K. Gehring, J.J. Bergeron, D.Y. Thomas, Protein quality control in the ER: the recognition of misfolded proteins, Semin. Cell Dev. Biol. 21 (2010) 500–511.
[9] D.T. Rutkowski, R.J. Kaufman, A trip to the ER: coping with stress, Trends Cell Biol. 14 (2004) 20–28.
[10] A. Bertolotti, Y. Zhang, L.M. Hendershot, H.P. Harding, D. Ron, Dynamic interaction of BiP and ER stress transducers in the unfolded-protein response, Nat. Cell Biol. 2 (2000) 326–332.
[11] M. Sallese, M. Giannotta, A. Luini, Coordination of the secretory compartments via inter-organelle signalling, Semin. Cell Dev. Biol. 20 (2009) 801–809.
[12] J. Shen, X. Chen, L. Hendershot, R. Prywes, ER stress regulation of ATF6 localization by dissociation of BiP/GRP78 binding and unmasking of Golgi localization signals, Dev. Cell 3 (2002) 99–111.
[13] E. Spear, D.T. Ng, The unfolded protein response: no longer just a special teams player, Traffic 2 (2001) 515–523.
[14] H. Yoshida, T. Matsui, A. Yamamoto, T. Okada, K. Mori, XBP1 mRNA is induced by ATF6 and spliced by IRE1 in response to ER stress to produce a highly active transcription factor, Cell 107 (2001).
[15] M. Ogata, S. Hino, A. Saito, K. Morikawa, S. Kondo, S. Kanemoto, T. Murakami, M. Taniguchi, I. Tanii, K. Yoshinaga, S. Shiosaka, J.A. Hammarback, F. Urano, K. Imaizumi, Autophagy is activated for cell survival after endoplasmic reticulum stress, Mol. Cell. Biol. 26 (2006) 9220–9231.
[16] R. Iurlaro, C. Munoz-Pinedo, Cell death induced by endoplasmic reticulum stress, FEBS J. 283 (2016) 2640–2652.
[17] K. Lee, W. Tirasophon, X. Shen, M. Michalak, R. Prywes, T. Okada, H. Yoshida, K. Mori, R.J. Kaufman, IRE1-mediated unconventional mRNA splicing and S2P-mediated ATF6 cleavage merge to regulate XBP1 in signaling the unfolded protein response, Genes Dev. 16 (2002).
[18] L. Zhao, C. Longo-Guess, B.S. Harris, J.W. Lee, S.L. Ackerman, Protein accumulation and neurodegeneration in the woozy mutant mouse is caused by disruption of SIL1, a cochaperone of BiP, Nat. Genet. 37 (2005) 974–979.
[19] A. Roos, S. Buchkremer, L. Kollipara, T. Labisch, C. Gatz, M. Zitzelsberger, E. Brauers, K. Nolte, J.M. Schroder, J. Kirschner, C.M. Jesse, H.H. Goebel, A. Goswami, R. Zimmermann, R.P. Zahedi, J. Senderek, J. Weis, Myopathy in Marinesco-Sjogren syndrome links endoplasmic reticulum chaperone dysfunction to nuclear envelope pathology, Acta Neuropathol. 127 (2014) 761–777.
[20] L. Zhao, C. Rosales, K. Seburn, D. Ron, S.L. Ackerman, Alteration of the unfolded protein response modifies neurodegeneration in a mouse model of Marinesco-Sjogren syndrome, Hum. Mol. Genet. 19 (2010) 25–35.
[21] A. Weitzmann, J. Volkmer, R. Zimmermann, The nucleotide exchange factor activity of Grp170 may explain the non-lethal phenotype of loss of Sil1 function in man and mouse, FEBS Lett. 580 (2006) 5237–5240.
[22] V.P. Ichhaporia, T. Sanford, J. Howes, T.N. Marion, L.M. Hendershot, Sil1, a nucleotide exchange factor for BiP, is not required for antibody assembly or secretion, Mol. Biol. Cell 26 (2015) 420–429.
[23] L. Kollipara, S. Buchkremer, J.A.G. Coraspe, D. Hathazi, J. Senderek, J. Weis, R.P. Zahedi, A. Roos, In-depth phenotyping of lymphoblastoid cells suggests selective cellular vulnerability in Marinesco-Sjogren syndrome, Oncotarget 8 (2017) 68493–68516.
[24] A. Roos, L. Kollipara, S. Buchkremer, T. Labisch, E. Brauers, C. Gatz, C. Lentz, J. Gerardo-Nava, J. Weis, R.P. Zahedi, Cellular signature of SIL1 depletion: disease pathogenesis due to alterations in protein composition beyond the ER machinery, Mol. Neurobiol. 53 (2016) 5527–5541.
[25] S. Lindal, I. Lund, T. Torbergsen, J. Aasly, S.I. Mellgren, O. Borud, P. Monstad, Mitochondrial diseases and myopathies: a series of muscle biopsy specimens with ultrastructural changes in the mitochondria, Ultrastruct. Pathol. 16 (1992) 263–275.
[26] K. Sasaki, K. Suga, S. Tsugawa, K. Sakuma, N. Tachi, S. Chiba, S. Imamura, Muscle pathology in Marinesco-Sjogren syndrome: a unique ultrastructural feature, Brain and Development 18 (1996) 64–67.
[27] C. Zimmer, G. Gosztonyi, J. Cervos-Navarro, A. von Moers, J.M. Schroder, Neuropathy with lysosomal changes in Marinesco-Sjogren syndrome: fine structural findings in skeletal muscle and conjunctiva, Neuropediatrics 23 (1992) 329–335.
[28] M. d'Avenia, R. Citro, M. De Marco, A. Veronese, A. Rosati, R. Visone, S. Leptidis, L. Philippen, G. Vitale, A. Cavallo, A. Silverio, C. Prota, P. Gravina, A. De Cola, E. Carletti, G. Coppola, S. Gallo, G. Provenza, E. Bossone, F. Piscione, M. Hahne, L.J. De Windt, M.C. Turco, V. De Laurenzi, A novel miR-371a-5p-mediated pathway, leading to BAG3 upregulation in cardiomyocytes in response to epinephrine, is lost in Takotsubo cardiomyopathy, Cell Death Dis. 6 (2015) e1948.
[29] T. Pulvirenti, M. Giannotta, M. Capestrano, M. Capitani, A. Pisanu, R.S. Polishchuk, E. San Pietro, G.V. Beznoussenko, A.A. Mironov, G. Turacchio, V.W. Hsu, M. Sallese, A. Luini, A traffic-activated Golgi-based signalling circuit coordinates the secretory pathway, Nat. Cell Biol. 10 (2008) 912–922.
[30] E.M.M. Manders, F.J. Verbeek, J.A. Aten, Measurement of colocalization of objects in dual-color confocal images, J. Microsc. 169 (1993) 375–382.
[31] H.P. Hauri, F. Kappeler, H. Andersson, C. Appenzeller, ERGIC-53 and traffic in the secretory pathway, J. Cell Sci. 113 (Pt 4) (2000) 587–596.
[32] S.Y. Qin, N. Kawasaki, D. Hu, H. Tozawa, N. Matsumoto, K. Yamamoto, Subcellular localization of ERGIC-53 under endoplasmic reticulum stress condition, Glycobiology 22 (2012) 1709–1720.
[33] S. Sur, M.O. Guler, M.J. Webber, E.T. Pashuck, M. Ito, S.I. Stupp, T. Launey, Synergistic regulation of cerebellar Purkinje neuron development by laminin epitopes and collagen on an artificial hybrid matrix construct, Biomater. Sci. 2 (2014) 903–914.
[34] M. Halliday, H. Radford, K.A.M. Zents, C. Molloy, J.A. Moreno, N.C. Verity, E. Smith, C.A. Ortori, D.A. Barrett, M. Bushell, G.R. Mallucci, Repurposed drugs targeting eIF2alpha-P-mediated translational repression prevent neurodegeneration in mice, Brain 140 (2017) 1768–1783.
[35] H. Radford, J.A. Moreno, N. Verity, M. Halliday, G.R. Mallucci, PERK inhibition prevents tau-mediated neurodegeneration in a mouse model of frontotemporal dementia, Acta Neuropathol. 130 (2015) 633–642.
[36] H.L. Smith, G.R. Mallucci, The unfolded protein response: mechanisms and therapy of neurodegeneration, Brain 139 (2016) 2113–2121.
[37] J.A. Moreno, M. Halliday, C. Molloy, H. Radford, N. Verity, J.M. Axten, C.A. Ortori, A.E. Willis, P.M. Fischer, D.A. Barrett, G.R. Mallucci, Oral treatment targeting the unfolded protein response prevents neurodegeneration and clinical disease in prion-infected mice, Sci. Transl. Med. 5 (2013) 206ra138.
[38] A. Filezac De L'Etang, N. Maharjan, M. Cordeiro Brana, C. Ruegsegger, R. Rehmann, A. Goswami, A. Roos, D. Troost, B.L. Schneider, J. Weis, S. Saxena, Marinesco-Sjogren syndrome protein SIL1 regulates motor neuron subtype-selective ER stress in ALS, Nat. Neurosci. 18 (2015) 227–238.
[39] P. Hu, Z. Han, A.D. Couvillon, R.J. Kaufman, J.H. Exton, Autocrine tumor necrosis factor alpha links endoplasmic reticulum stress to the membrane death receptor pathway through IRE1alpha-mediated NF-kappaB activation and down-regulation of TRAF2 expression, Mol. Cell. Biol. 26 (2006) 3071–3084.
[40] M. Giannotta, C. Ruggiero, M. Grossi, J. Cancino, M. Capitani, T. Pulvirenti, G.M. Consoli, C. Geraci, F. Fanelli, A. Luini, M. Sallese, The KDEL receptor couples

to Galphaq/11 to activate Src kinases and regulate transport through the Golgi, EMBO J. 31 (2012) 2869–2881.
[41] C. Liu, M. Mei, Q. Li, P. Roboti, Q. Pang, Z. Ying, F. Gao, M. Lowe, S. Bao, Loss of the golgin GM130 causes Golgi disruption, Purkinje neuron loss, and ataxia in mice, Proc. Natl. Acad. Sci. U. S. A. 114 (2017) 346–351.
[42] Y. Inaguma, N. Hamada, H. Tabata, I. Iwamoto, M. Mizuno, Y.V. Nishimura, H. Ito, R. Morishita, M. Suzuki, K. Ohno, T. Kumagai, K. Nagata, SIL1, a causative co-chaperone gene of Marinesco-Sojgren syndrome, plays an essential role in establishing the architecture of the developing cerebral cortex, EMBO Mol. Med. 6 (2014) 414–429.
[43] J.A. Moreno, H. Radford, D. Peretti, J.R. Steinert, N. Verity, M.G. Martin, M. Halliday, J. Morgan, D. Dinsdale, C.A. Ortori, D.A. Barrett, P. Tsaytler, A. Bertolotti, A.E. Willis, M. Bushell, G.R. Mallucci, Sustained translational repression by eIF2alpha-P mediates prion neurodegeneration, Nature 485 (2012) 507–511.
[44] T.K. Rainbolt, J.M. Saunders, R.L. Wiseman, Stress-responsive regulation of mitochondria through the ER unfolded protein response, Trends Endocrinol. Metab. 25 (2014) 528–537.
[45] Z. Liu, Y. Lv, N. Zhao, G. Guan, J. Wang, Protein kinase R-like ER kinase and its role in endoplasmic reticulum stress-decided cell fate, Cell Death Dis. 6 (2015) e1822.
[46] D. Rojas-Rivera, T. Delvaeye, R. Roelandt, W. Nerinckx, K. Augustyns, P. Vandenabeele, M.J.M. Bertrand, When PERK inhibitors turn out to be new potent RIPK1 inhibitors: critical issues on the specificity and use of GSK2606414 and GSK2656157, Cell Death Differ. 24 (2017) 1100–1110.
[47] V. Grande, F. Ornaghi, L. Comerio, E. Restelli, A. Masone, A. Corbelli, D. Tolomeo, V. Capone, J.M. Axten, N.J. Laping, F. Fiordaliso, M. Sallese, R. Chiesa, PERK inhibition delays neurodegeneration and improves motor function in a mouse model of Marinesco-Sjogren syndrome, Hum. Mol. Genet. 27 (2018) 2477–2489 https://academic.oup.com/hmg/article-abstract/27/14/2477/4990255?redirectedFrom=fulltext.